Lasers in Eng., Vol. 41, pp. 111–128
Reprints available directly from the publisher
Photocopying permitted by license only

Thermal Fatigue Behaviour of Cast Iron Induced by Pulse Laser Heating: Numerical Simulation and Experimental Studies

H. LIU[1,2,*], P-J. CHEN[3], J-B. HAO[1], H-F. YANG[1], X-L. HE[4] AND G. YU[4]

[1]*School of Mechanical and Electrical Engineering, China University of Mining and Technology, Xuzhou 221116, Jiangsu Province, China*
[2]*Jiangsu Key Laboratory of Mine Mechanical and Electrical Equipment, China University of Mining & Technology, Xuzhou 221116, Jiangsu Province, China*
[3]*School of Mechanics and Civil Engineering, China University of Mining and Technology, Xuzhou 221116, Jiangsu Province, China*
[4]*Key Laboratory of Mechanics in Advanced Manufacturing, Institute of Mechanics, Chinese Academy of Science, Beijing, China*

Thermal fatigue is one of the key damage mechanisms in components suffering high temperature cycles. To shorten the duration of a thermal fatigue test and improve its reliability, apparatus was designed using a laser as the heat source, considering the good controllability and high energy density of a laser in both time and space. The temperature and stress fields induced by a laser under high temperature cycling were investigated by a coupled thermo-mechanical finite element method (FEM) model. Results show that, under the cyclic action of the laser, pulse compressive stresses were produced and were non-uniformly distributed on the cast iron surface, providing essential conditions for cracking. After 1000 thermal cycles, network cracks occurred on the surface area irradiated by the laser. It is believed that the cracks initiated from holes formed by the spalling of graphite, and propagated to connect with each other under the effects of the pulsed compressive stresses.

Keywords: Nd:YAG laser, cast iron, cracking, thermal fatigue, temperature field, numerical model, finite element method (FEM)

*Corresponding author: Tel: +86 (0)152 5203 6516; E-mail: liuhao56@cumt.edu.cn

1 INTRODUCTION

A large number of components suffering high temperature cycles are widely used in engines, steam turbines, nuclear reactors, and in casting and forging equipment; thermal fatigue is one of the common causes of failure of these types of components. Understanding the mechanisms of thermal fatigue and improving thermal fatigue resistance is key to prolonging the service life of such components.

Numerous researchers have conducted experiments and numerical studies on the thermal fatigue behaviour of many materials. By using flame heating method, Birol *et al.* [1] tested the thermal fatigue resistances of three alloys including X32CrMoV33 steel, Inconel 617 and Stellite 6. According to the results, Inconel 617 and Stellite 6 presented a superior resistance to thermal fatigue cracking, owing to their better resistances to oxidation and temper-softening than those of X32CrMoV33 steel. By using the same experimental method, Birol *et al.* [2] analysed the thermal fatigue performances of Stellite 6 coatings deposited through plasma transfer arc-welding. Persson *et al.* [3] designed apparatus that could simulate thermal fatigue and used it to perform cyclic induction heating and interior cooling of hollow cylinder test rods and a laser speckle technique was used to record surface strains in a thermal cycling process. Jia *et al.* [4] confirmed that specimens with bionic surfaces with striation- and diamond-shape morphologies had better thermal fatigue behaviour than untreated specimens. Mellouli *et al.* [5] revealed the influences of microstructure and chemical composition on the cracking behaviour of various cast irons under thermal cycling induced by focused halogen lamp radiation. Xu *et al.* [6] estimated the effects of two surface modification technologies including laser deep penetration spot cladding, and brush plating, on the thermal fatigue properties of Cr12MoNi hot-working die steels. In the experiment, rapid heating was realised by electric resistance furnaces. By utilising this experimental method for self-controlling thermal fatigue, Cong *et al.* [7] tested the thermal fatigue resistance of hot-working die steel repaired by partial laser surface remelting and an alloying process. Their test method also heated and cooled specimens by using electric furnaces and water, respectively. Tong *et al.* [8, 9], Zhang *et al.* [10], and Ning *et al.* [11] designed similar equipment and a comparable method to assess the thermal fatigue performance of cast iron with bionic surface, 3Cr2W8V die steels, and K125L superalloy, respectively.

Until now, due to the inherent complexity of thermal fatigue problems, there is no standard procedure and equipment available for thermal fatigue testing [12]. Among the established experimental apparatus, resistance furnaces are mostly used for sample heating; however, the temperature distribution on the surface of a specimen heated in a resistance furnace tends to be uniform, which differs significantly from that of components under actual working conditions. Thus, the thermal stress intensity caused by the temperature gradient at high temperatures decreases. In addition, another drawback is that it takes too long

to heat the specimen. Laser beams have the advantages of a high energy density and good controllability. The original laser beams applied to form a Gaussian distribution of energy can be transformed into those with arbitrary intensity distributions by use of optical elements [13]. When such laser beams are used to irradiate the surface of a component, temperature fields similar to those in actual working conditions can be obtained [14,15].

This study, therefore, designed test equipment involving the use of a laser as its heat source. In automotive industry, cast iron is widely used to manufacture cylinders, which suffer from severe and cyclic thermal load; consequently, the thermal fatigue behaviour of cast iron was evaluated using this equipment. Also, thermal and stress fields induced by pulsed laser heating were discussed based on a coupled thermo-mechanical transient FEM model, and the initiation and growth of cracks under thermal cycles were analysed.

2 EXPERIMENTAL APPARATUS AND DESIGN

As seen in Figure 1, the laser thermal fatigue experimental apparatus mainly consists of a laser, an air compressor, a nozzle, an infrared radiation thermometer, a thermocouple, a computer and a clamp. Laser beams at a wavelength of 1064 nm were emitted from a Nd:YAG continuous wave (CW) solid laser (HLD1001.5; Trumpf, GmbH) to irradiate the surface of each sample. In the cooling stage a high-pressure airflow generated in the air compressor (176-7; Shanghai Jiebao Compressor Manufacturing Company, Ltd.) was applied to the rear surface of each sample by a nozzle to strengthen the heat transfer effect thereon. The maximum and minimum, output powers of the laser were 1000 and 10 W, respectively. Laser energy was output in multi-mode hybrid fashion and the energy distributed as a flat topped profile. An optical fibre with a diameter of 0.15 mm was used to deliver laser beams to the laser head. Then, laser beams were transformed into parallel light beams through a collimating lens and were focused by a focusing lens.

The optical system and convergence characteristics of laser beams are shown in Figure 2. Here d_k is the diameter of the optical fibre, f_c is the focal length of the collimating lens, θ is the divergence angle before focusing d_0 is the diameter of the collimating beams, f is the focal length of the focusing lens, Z_R is the Rayleigh length, d_{0f} is the focusing diameter and θ_f is the divergence angle after focusing. Laser beams with different convergence characteristics can be obtained by using a focusing lens with different focal lengths, and the relationship between the focal length of the focusing lens and the characteristics of laser beams in this system is shown in Table 1.

In this experiment a focusing lens with a collimating focal length of 200 mm was used. Light spots required in this thermal fatigue experiment induced by laser heating were obtained by adjusting the defocusing distance which represents the

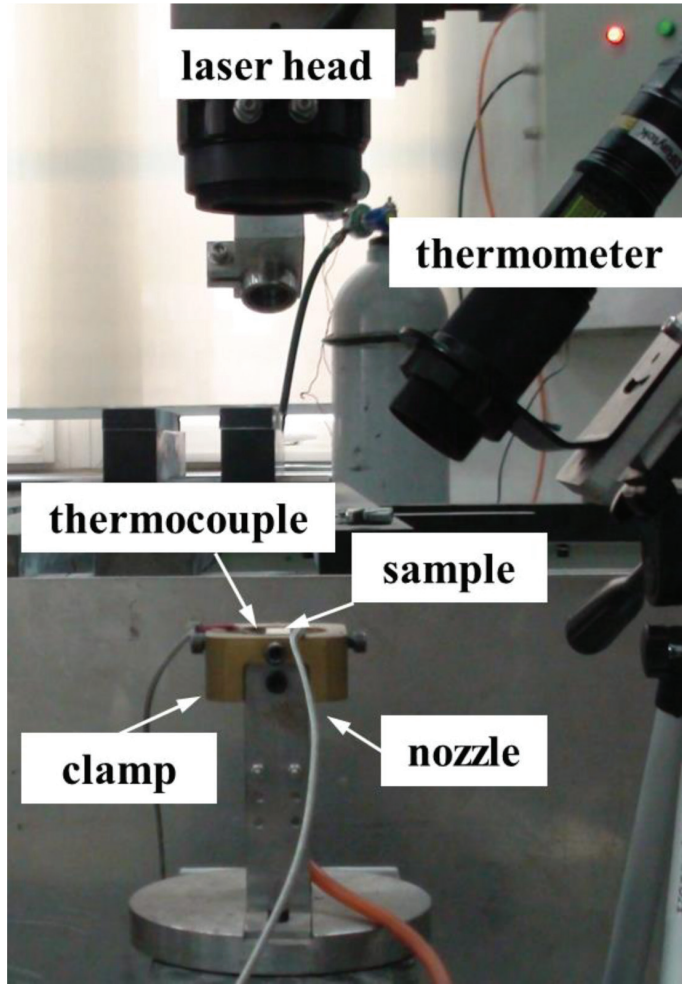

FIGURE 1
Photograph of the experimental apparatus for the thermal fatigue testing.

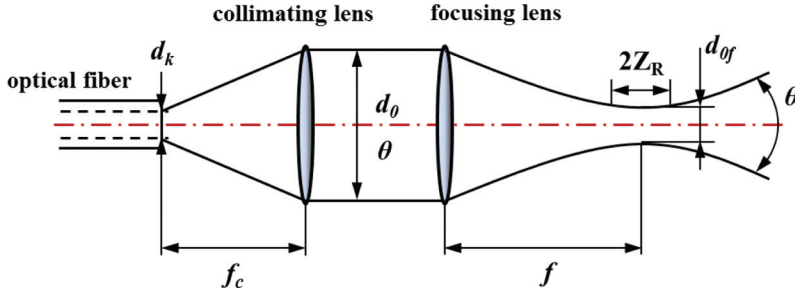

FIGURE 2
Schematic diagram optical system and laser beam characteristics.

TABLE 1
Characteristics of the Nd:YAG laser beams used in the apparatus.

f/mm	d_{0f} (mm)	Z_R (mm)
100.00	0.08	0.23
150.00	0.11	0.53
200.00	0.15	0.94

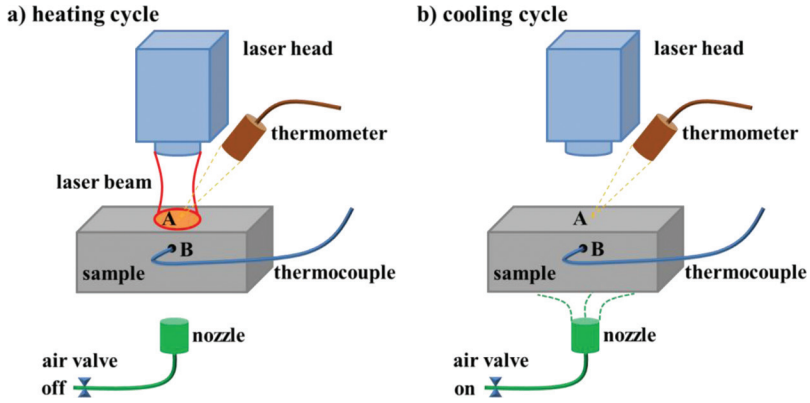

FIGURE 3
Sketches of the thermal fatigue test process showing (a) heating cycle and (b) cooling cycle.

distance between the laser focal plane and the sample surface. The relationship between the diameter of the light spots and the defocusing distance is

$$d(z) = d_{0f}\sqrt{1+(\frac{z}{Z_R})^2} \tag{1}$$

where, $d(z)$ denotes for the diameter of the light spots at defocusing distance z.

The cuboidal cast iron samples ($20 \times 10 \times 10\,\text{mm}^3$) and the nozzle were fixed on the clamp. The process of thermal fatigue testing, as induced here by laser heating, is shown in Figure 3. The infrared radiation thermometer (Marathon 2ML; Raytek Corporation) and the thermocouple (TC-08; Pico Technology, Ltd.) were used to record the temperature of the centre of the surface (Point A) of the sample and a specific point (Point B) on the side face of the sample, separately. The temperature data obtained by using the infrared radiation thermometer were used as programmed control signals, while those obtained from the thermocouple were used as comparative data for the simulation calculation and correction of material emissivity. Before the thermal

fatigue experiment, control parameters such as the laser power (P), upper and lower limit temperatures (T_{max} and T_{min}), and cycle times (N) were set. At the beginning of the experiment, the air valve was closed and the sample was heated by laser radiation. When the temperature at Point A reached the upper limit temperature, the laser was turned off immediately, while the valve was opened, thus beginning the cooling stage. Then the sample was cooled by the impinging airflow. When the temperature at Point A was lower than the set lower limit temperature, the laser was turned on and air valve was closed. The cycle continued and the thermal fatigue experiment stopped when the desired number of cycles had been reached.

3 RESULTS AND DISCUSSION

3.1 Characteristics of the thermal cycles

Cast iron was used to explore the experimental process and feasibility of thermal fatigue induced by laser heating. The cast iron sample was cut from the cylinder head of an automobile engine. The cylinder head was subjected to the thermal cycle load at a maximum temperature of 400°C when the engine was operating as normal. The upper limit temperature of each thermal cycle has a key effect on the extent of thermal fatigue damage. Mellouli *et al.* [5] found that increasing the maximum temperature of thermal cycles not only significantly shortens the time to crack initiation, but also increases the number and growth rate of cracks. So, to shorten the cycle times of this thermal fatigue experiment, and improve the experimental efficiency, the upper limit temperature of the thermal cycle can be improved; however, the upper limit temperature should be controlled so as to always remain below the phase transformation temperature of the sample under test, so as to avoid a solid-state phase transition, and even melting of the material. According to these principles, the upper limit temperature of the thermal fatigue experiment of cast irons was set at 575°C. The parameters used in the thermal fatigue testing of cast iron induced by laser heating are shown in Table 2.

Figure 4 shows the laser power curves in the middle of the experiment and temperature curves obtained from the infrared radiation thermometer. During the experiment, after being controlled, the continuous laser was modulated into pulse outputs, and the pulse width and the cycle of laser pulses corresponded to the heating phase and the period of the temperature cyclic curve.

TABLE 2
The parameters used in the thermal fatigue testing of cast iron induced by laser heating.

T_{max} (°C)	T_{min} (°C)	N	P (W)	*d* (mm)
575	300	1000	500	8.00

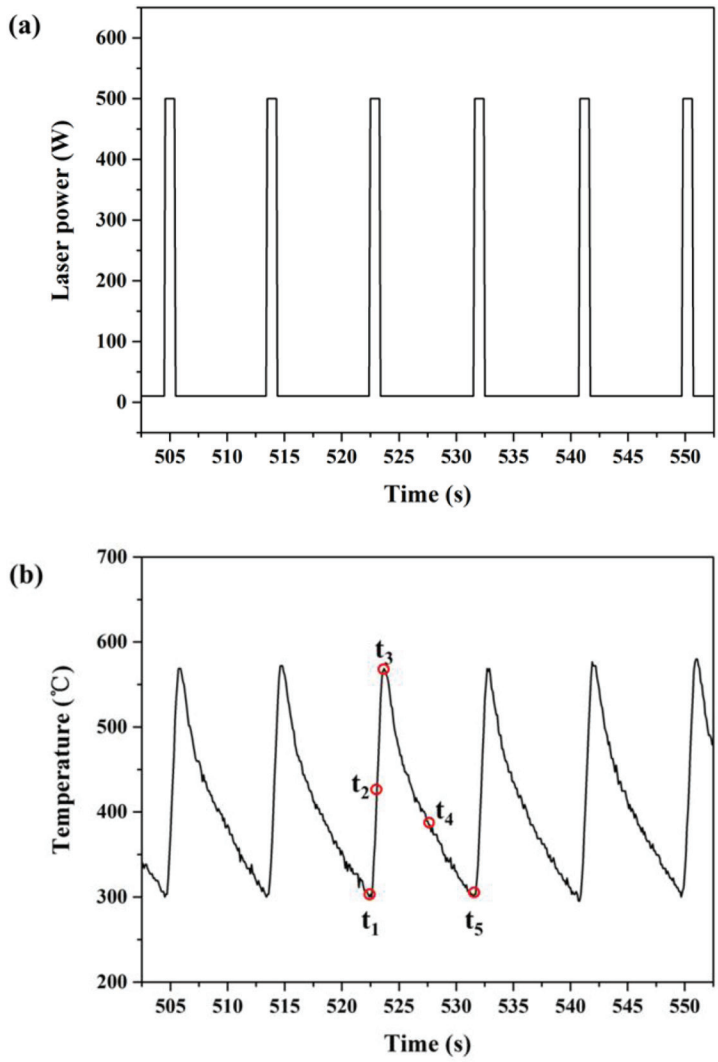

FIGURE 4
Thermal fatigue cycles for (a) Nd:YAG laser power and (b) temperature recorded by pyrometer.

The temperature cyclic curve was composed of similar thermal cycles, each of which was divided into heating and cooling stages. In addition, the period of a thermal cycle was 8.8 seconds, in which the heating and cooling time durations were about 0.9 and 7.9 seconds, respectively. Compared with the thermal fatigue experiments undertaken using electric resistance furnaces and electromagnetic induction as heating methods, the length of the thermal cycles achieved in this research was significantly decreased; thus shortening the duration of each experiment.

3.2 Thermal and stress analysis

To study further the temperature and thermal stress fields in a thermal cycle, a thermo-mechanical coupled transient FEM model was established. In the interaction between the laser and the material, the energy of the metal increased as the free electrons in the metal absorbed photons and was then delivered to lattices in the interior of the material through electron collision. Due to the extremely short relaxation time (the characteristic time was 10^{-13} seconds) of the collision between electrons and lattices, it was thought that the laser energy absorbed by the metal was instantaneously transformed into thermal energy. Owing to the large density of free electrons in the metal, the laser energy was absorbed in an extremely thin layer. The thin layer absorbing the laser energy was rapidly heated, and the heat was transported to the interior by conduction; therefore, the heat conduction equation based on Fourier's laws was adopted in the numerical model. The governing equation for the conservation of energy to calculate the transient temperature distribution $T(x, y, z, t)$ was expressed as

$$\frac{\partial(\rho c T)}{\partial t} = \frac{\partial}{\partial x}\left(k\frac{\partial T}{\partial x}\right) + \frac{\partial}{\partial y}\left(k\frac{\partial T}{\partial y}\right) + \frac{\partial}{\partial z}\left(k\frac{\partial T}{\partial z}\right) \tag{2}$$

where k represented thermal conductivity, ρ represented material density, c represented specific heat capacity and t represented time. Thermal stresses were produced due to the non-uniform temperature field, and was expressed as

$$\sigma = E\alpha\Delta T \tag{3}$$

where σ is the thermal stress, E is the elasticity modulus, α is the coefficient of linear expansion and ΔT is the variation of temperature. The initial temperature was set at room temperature:

$$T(x, y, z)\big|_{t=0} = T_a \tag{4}$$

where T_a represented the ambient temperature. At the boundary of the sample, an integrated heat dissipation coefficient was used to describe the thermal convection and radiation of metal surfaces, so as to reduce the degree of nonlinearity of the solutions [16]. This coefficient and the boundary conditions could be expressed as

$$h_c = 2.41\times10^{-3}\varepsilon T^{1.61} \tag{5}$$

and

$$k\left(\nabla T\cdot\mathbf{n}\right)\Big|_s = -h_c\left(T-T_a\right)_s \quad \text{if } S\notin\Omega \tag{6}$$

where ε was the emissivity, **n** was the normal vector of the surface, S represented the sample surfaces and Ω represented the area where the laser beam radiated. In the FEM model a uniform surface heat source was applied to simulate the energy input by the laser beam:

$$q(r) = \frac{4aP}{\pi d^2} \quad \text{if } S\in\Omega \tag{7}$$

where a was absorptivity and P was the laser power. The displacements of two side surfaces were restricted because of the fixation by the clamp.

In accordance with the sample size a geometric model was established and mesh-generation using hexahedral elements with eight nodes undertaken (see Figure 5). The origin of the original coordinate system was located on the short side on the top surface of the sample, and the x- and y-axes indicated the

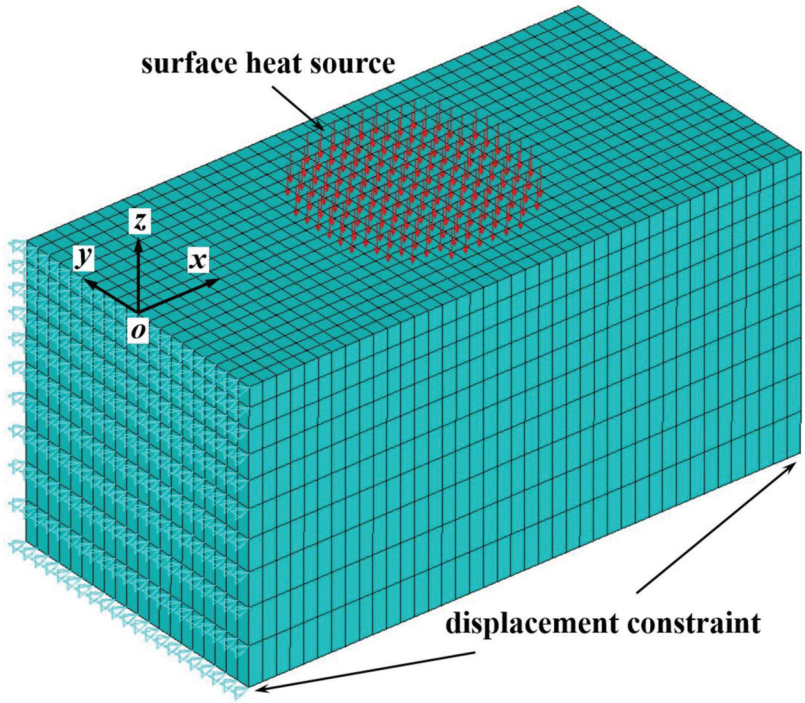

FIGURE 5
Finite element (FE) mesh and geometry showing the surface heat source and displacement constraint.

TABLE 3
Chemical composition of cast iron (wt.%) used in this work.

C	Si	Mn	P	S	Fe
3.600	2.700	0.200	0.046	0.017	Bal.

TABLE 4
Material properties of cast iron used in the model.

Temperature (°C)	20	400	600	800	1000
Thermal conductivity (W/mK)	39.17	34.38	30.86	29.20	28.04
Specific heat capacity (J/kgK)	513	620	734	789	723
Elasticity modulus (GPa)	115.0	104.0	95.1	73.9	56.1
Linear expansion coefficient(10^{-5} K^{-1})	1.20	2.20	3.35	4.50	5.70
Poisson ratio	0.24	0.31	0.34	0.28	0.26

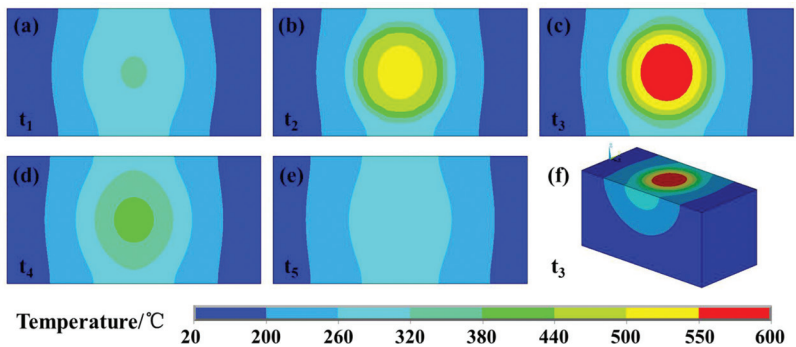

FIGURE 6
Plots showing the temperature distribution at different times of a thermal cycle.

length and width directions of the sample, respectively, while the *z*-axis represented the outer normal to the top surface. There were 8000 brick elements in total, each with a length 0.50 mm and a width of 0.50 mm. The geometric model was divided into 10 layers of elements, which were finer in the vicinity of top surface. Chemical composition and thermal properties of cast iron used in this model are shown in Table 3 and Table 4, respectively[17,18]. The model was validated by our previous work [19].

Figure 6 shows the temperature distribution at different time points of a thermal cycle in the middle stage of the thermal fatigue test, and the temperature field was calculated based on the FEM model. Figure 4 shows the time points represented by t_1, to t_5: because of the effects of previous thermal cycles, at the beginning of heating time t_1 of this thermal cycle, the tempera-

ture in the sample was distributed in a non-uniform fashion and the highest temperature was found on the surface at the centre of the sample. Under laser irradiation (t_1 to t_3), the temperature at the centre of the surface of the sample increased rapidly, and the radial temperature gradient in the region within the radius of the laser beams also increased to a significant extent. During the cooling phase (t_3 to t_5), the heat was conducted into the interior and dissipated to the environment under the influence of the applied airflow, so the temperature of the sample, as well as the temperature gradient, gradually decreased. At the end of cooling time t_5, the temperature was distributed in a manner similar to that at the beginning time of the thermal cycle (at t_1). Figure 7 shows the temperature distribution along the depth direction of the sample at its centre. In a thermal cycle, the layer within a depth of 3 mm beneath the sample surface was subjected to large thermal shocks, while below this region, and to the bottom of the sample, the temperature distribution within a given thermal cycle remained almost unchanged. These trends indicated that the test sample was in dynamic thermal equilibrium during this laser-induced thermal fatigue test.

As the centre of the top surface was at a higher temperature, material in the vicinity tended to expand: the temperature around the centre of the sample decreased rapidly, leading to the expansion of the centre of the sample

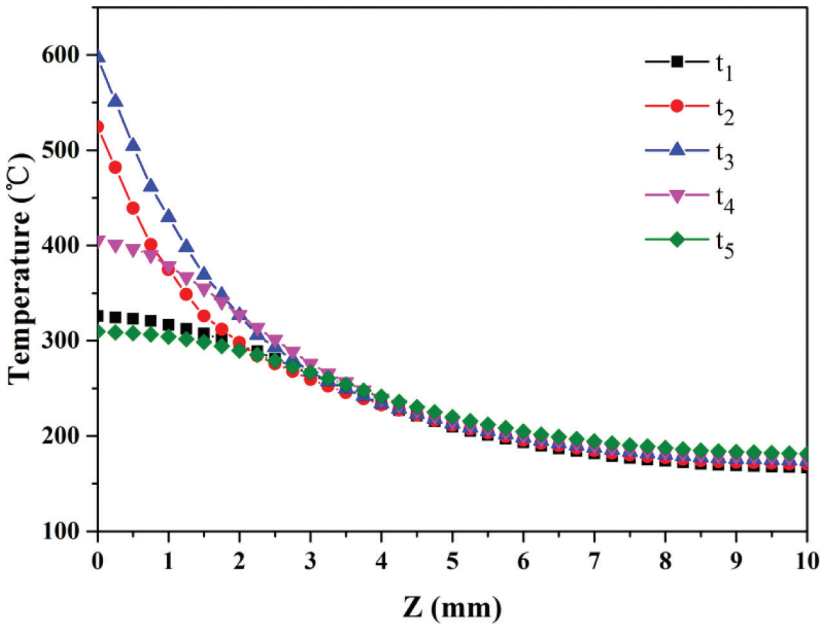

FIGUR E 7
Graph showing the temperature profiles along the depth direction at different times of a thermal cycle.

surfaces being restricted by the presence of the surrounding material, so the centre of the surface was subjected to compressive stresses. The compressive stresses were produced by the temperature gradient, and the larger the temperature gradient, the greater the compressive stress [6]. Due to the symmetry of the sample, the stress level change within a thermal cycle was assessed by taking the thermal stress in the x-direction (the x-component stress in the stress tensor under the global coordinate) as an example. Figure 8(a) and Figure 8(b) show the profiles of thermal stress along the x- and z-axes. At the beginning of the heating cycle, stresses were distributed uniformly, and the compressive stress at the centre of the pulsed laser was slightly lower. With increased laser irradiation time, the compressive stresses in the centre increased rapidly. At the moment when the laser was turned off, the maximum compressive stress increased threefold. In the cooling stage, the compressive stresses gradually returned to their initial level. The amplitude of compressive stress along the x-axis in any given thermal cycle decreased with increasing distance from the centre. The compressive stresses fluctuated in the region bounded by $2.00\,\text{mm} < x < 18.00\,\text{mm}$, indicating where cracks were most likely to occur. It can be seen from Figure 8(b) that the fluctuation of stresses was restricted to a thin layer (3.00 mm thick) near the surface. It was worth noting that, in the cooling stage, which occupied the majority of the period of each thermal cycle, the locus of the maximum compressive stress was inside the material rather than on its surface. The numerical results indicated that, under the effects of laser irradiation, pulsed compressive stresses were produced and distributed in a non-uniform fashion on the surface, which was a necessary condition for the initiation of thermal fatigue cracking.

3.3 Analysis of the thermal fatigue cracking

Optical microscope image of the sample surface before thermal fatigue testing is shown in Figure 9. The cast iron samples were mainly composed of a metal matrix and strip graphite; the length of the strip graphite components ranged from 10 to 200 μm.

After 1000 thermal cycles, the sample surface was observed under an optical microscope and the surface states from the centre to the edge of the samples are shown in Figure 10. Figure 10(a) shows the region located at $x = 10.00$ mm, and Figure 10(b) is the enlarged map of Figure 10(a). In addition, x-values of 12.00, 14.00, 16.00 and 18.00 mm are plotted, respectively, in Figures 10(c) to (f). In the area irradiated by the laser (see Figures 10(a) to (d)), obvious microcracks were detected, which extended linearly in a direction similar to that of the strip graphite. While strip graphite was not found in this area, revealing that the graphite was oxidized and converted into CO_2 in the thermal fatigue test. It was observed that warping occurred in the vicinity of the junction of reticular cracks. In addition, in the periphery of those laser irradiated regions (see Figure 10(e)), microcracks were not detected; however, it

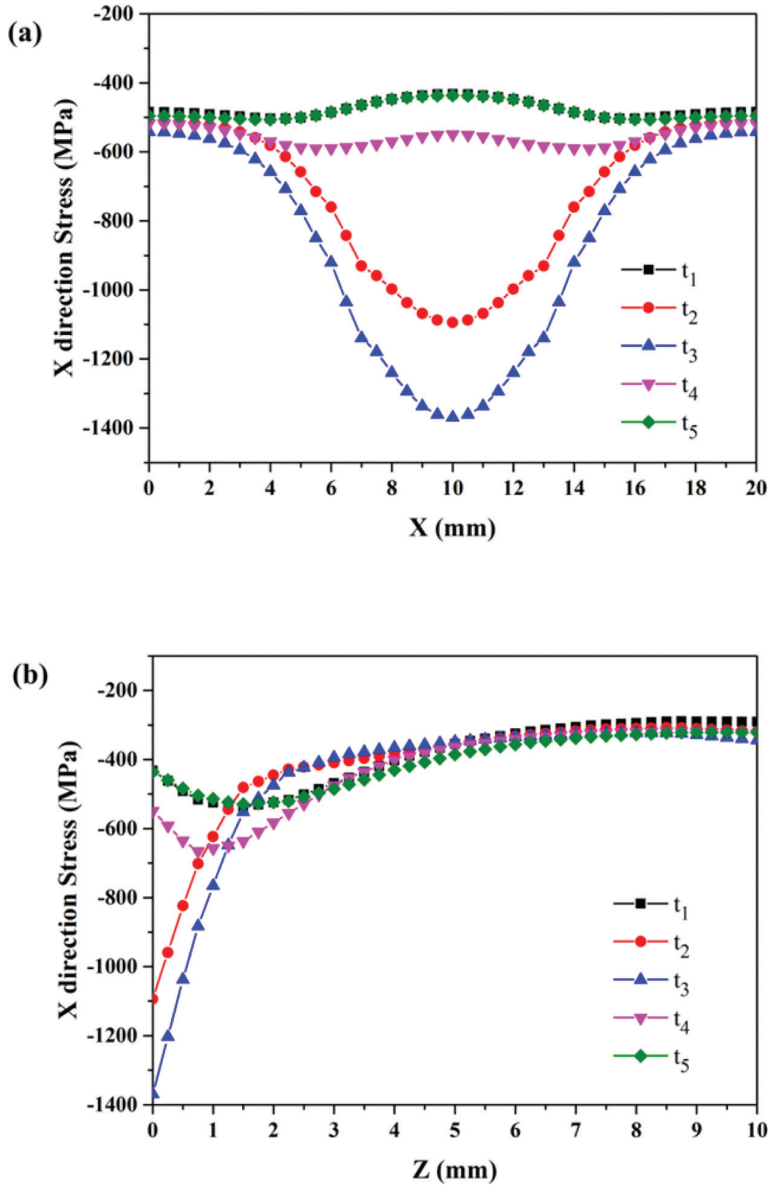

FIGURE 8
Graphs showing the *x*-direction stress curves (a) along the length direction and (b) the depth direction.

was found that the strip graphite disappeared in certain localised areas, which gradually became vacancy sites forming potential crack sources. At these positions, significant colour changes on material surfaces were observed, indicating that the metal matrix was oxidized under the action of thermal

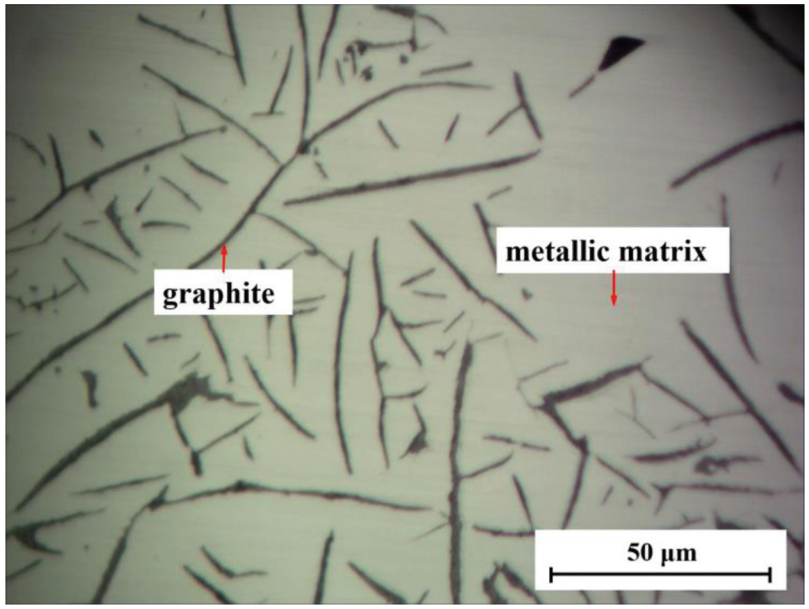

FIGURE 9
Optical micrograph showing the surface of the sample before thermal fatigue testing.

cycling and produced oxides including Fe_2O_3 and Fe_3O_4. In areas furthest from the incident laser radiation (see Figure 10(f)), after cessation of thermal fatigue cycles, microcracks were not found and the strip graphite remained intact, with the colour of the surface changing slightly. Figure 10 shows that, in the laser-induced thermal fatigue testing, the thermal shocks and stresses in different locations were distinct and significant differences were manifest on the sample surfaces. In conclusion, thermal fatigue cracks mainly occurred in laser irradiated areas, resulting from the high temperature and thermal stress levels experienced. In addition, owing to the high temperature, surfaces outside the laser irradiated areas were also oxidized.

The thermal fatigue of cast iron was the combined result of chemical corrosion (oxidation) and physical damage. On the surface of the cast iron samples, the vacancies, and holes, left in the metal matrix, resulting from the burning and removal of graphite, were the sources of fatigue cracks. During thermal cycling, because of the different thermal expansion coefficients of the metal matrix and the graphite, an uncoordinated strain occurred at the interface between the strip graphite and the metal matrix, thus stripping the graphite from its original position. Owing to the highest temperature of thermal recycling being much lower than the melting point of graphite, the removal of graphite could be regarded as the main means by which holes were produced, rather than the burning of graphite. Base on research by Mellouli *et al.* [5], at high temperatures, surface oxide layers with thicknesses

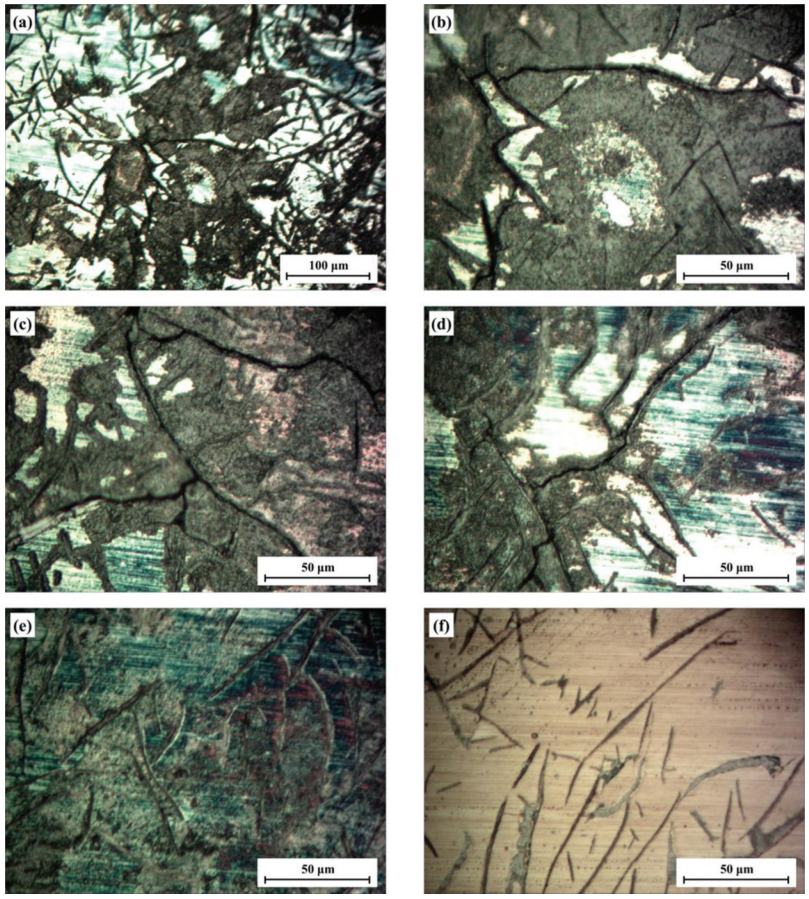

FIGURE 10
Optical micrographs showing the surface of different locations after 1000 times thermal fatigue cycles when (a) $x = 10.00$ mm, (b) magnified view of (a), (c) $x = 12.00$ mm, (d) $x = 14.00$ mm, (e) $x = 16.00$ mm and (f) $x = 18.00$ mm.

ranging from 50 μm to 200 μm are produced in cast iron samples according to their different compositions. The oxidation of the surface of cast iron samples led to a decrease in the local mechanical properties thereof, which impaired its ability to hinder crack growth. Under the pulsed compressive stresses induced by pulsed laser irradiation, crack tips developed constantly, together with other cracks, to form reticular fatigue cracks. Cracks also extended to the interior of the material. Due to the large strain in the crack convergence zone, surface warping was also observed. According to the numerical simulation results, the maximum stress was located below the top surface. It can be inferred that, if laser irradiation of the cast iron surface were to have been continued, lamellar spalling would have been likely to have occurred in regions of local crack closure.

4 CONCLUSIONS

This study designed new thermal fatigue test equipment and established a coupled thermo-mechanical finite element method (FEM) model capable of analysing the thermal and stress fields therein. Furthermore, the thermal fatigue properties of cast iron were tested. By using the laser thermal fatigue equipment, a thermal cycle with a minimum and maximum temperature of 300 and 575°C, respectively, was constructed. The period of a single thermal cycle was only 8.8 seconds, meaning that the efficiency of thermal fatigue testing was improved significantly, compared with that of a test using an electric resistance furnace. Under the action of a pulsed Nd:YAG laser beam, pulsed compressive stresses were produced which were distributed in a non-uniform fashion on the sample surface. The compressive stress amplitudes decreased with increasing distance from the centre. After 1000 thermal cycles, reticular cracks were generated on the surfaces of the cast iron samples in laser-irradiated areas. Considering the shapes of these cracks, it was inferred that cracks initiated from the holes formed by the removal of graphite particles. Under the effects of pulsed compressive stresses, the cracks propagated and interconnected to form a network. The research shows that pulsed laser heating can be used to assess the thermal fatigue properties and analyse the cracking mechanisms of cast iron.

ACKNOWLEDGMENTS

The authors acknowledge the Fundamental Research Funds for the Central Universities (2017QNA18) and the Project Funded by Priority Academic Program Development of Jiangsu Higher Education Institutions (PAPD).

NOMENCLATURE

a	Absorptivity
c	Specific heat capacity (J/kgK)
d	Laser beam diameter at the sample surface (mm)
d_0	Diameter of the collimating beams (mm)
d_{0f}	Focusing diameter (mm)
d_k	Diameter of optical fibre (mm)
$d(z)$	Diameter of the light spots at defocusing distance z (mm)
E	Elasticity modulus (GPa)
f	Focal length of the focusing lens (mm)

f_c Focal length of the collimating lens (mm)
h_c Integrated heat dissipation coefficient
k Thermal conductivity (W/mK)
N Cycle times
P Laser power (W)
q Laser energy density (W/mm^2)
S Surface area (mm^2)
T Temperature (°C)
T_a Ambient temperature (°C)
T_{max} Upper limit temperatures (°C)
T_{min} Lower limit temperatures (°C)
ΔT Variation of temperature (°C)
t Time (seconds)
Z_R The Rayleigh length (mm)
z Defocusing distance (mm)

Greek symbols

α Coefficient of linear expansion (K^{-1})
ε Emissivity
θ Divergence angle before focusing
θ_f Divergence angle after focusing
ρ Material density (kg/m^3)
σ Thermal stress (MPa)
Ω Laser beam radiated area (mm^2)

REFERENCES

[1] Birol Y. Thermal fatigue testing of Inconel 617 and Stellite 6 alloys as potential tooling materials for thixoforming of steels. *Materials Science & Engineering A. Structural Materials: Properties, Microstructure and Processing* **527**(7-8) (2010), 1938–1945.

[2] Birol Y. Thermal fatigue testing of Stellite 6-coated hot work tool steel. *Materials Science & Engineering A. Structural Materials: Properties, Microstructure and Processing* **527**(21–22) (2010), 6091–6097.

[3] Persson A., Hogmark S. and Bergström J. Simulation and evaluation of thermal fatigue cracking of hot work tool steels. *International Journal of Fatigue* **26**(10) (2004), 1095–1107.

[4] Jia Z.X., Liu Y.W., Li J.Q., Liu L.J. and Li H.L. Crack growth behavior at thermal fatigue of H13 tool steel processed by laser surface melting. *International Journal of Fatigue* **78** (2015), 61–71.

[5] Mellouli D., Haddar N., Köster A. and Toure M.L. Thermal fatigue of cast irons for automotive application. *Materials & Design* **32**(3) (2011), 1508–1514.
[6] Xu J., Li Z., Zhu W., Liu Z. and Liu W. The comparative study of thermal fatigue behavior of laser deep penetration spot cladding coating and brush plating Ni–W–Co coating. *Applied Surface Science* **253**(5) (2006), 2618–2624.
[7] Cong D., Zhou H., Ren Z., Zhang H., Ren L., Meng C. and Wang C. Thermal fatigue resistance of hot work die steel repaired by partial laser surface remelting and alloying process. *Optics & Lasers in Engineering* **54**(1) (2014), 55–61.
[8] Tong X., Zhou H., Ren L., Zhang Z., Zhang W. and Cui R. Effects of graphite shape on thermal fatigue resistance of cast iron with biomimetic non-smooth surface. *International Journal of Fatigue* **31**(4) (2009), 668–677.
[9] Tong X., Li F.H., Liu M., Dai M.J. and Zhou H. Thermal fatigue resistance of non-smooth cast iron treated by laser cladding with different self-fluxing alloys. *Optics & Laser Technology* **42**(7) (2010), 1154–1161.
[10] Zhang Z., Zhou H., Ren L., Tong X., Shan H. and Liu L. Effect of units in different sizes on thermal fatigue behavior of 3Cr2W8V die steel with biomimetic non-smooth surface. *International Journal of Fatigue* **31**(3) (2009), 468–475.
[11] Ning, L.K., Zheng Z., An F.Q., Tang S., Tong J., Ji H.S. and Yu H.W. Thermal fatigue behavior of K125L superalloy. *Rare Metals* **35**(2) (2016), 172–176.
[12] Qayyum F., Shah M., Shakeel O., Mukhtar F., Salem M. and Rezai-Aria F. Numerical simulation of thermal fatigue behavior in a cracked disc of AISI H-11 tool steel. *Engineering Failure Analysis* **62** (2016), 242–253.
[13] Li S.X., Yu G., Zheng C.Y. and Tan Q.F. Duasi-Dammann grating with proportional intensity array spots. *Optics Letters* **33**(18) (2008), 2023–2025.
[14] Song H.W., Yu G., Tan J.S., Zhou L. and Yu X.L. Thermal fatigue on pistons induced by shaped high power laser. Part I: Experimental study of transient temperature field and temperature oscillation. *International Journal of Heat and Mass Transfer* **51**(3-4) (2008), 757–767.
[15] Song H.W., Yu G., Kaplan A.F.H., Tan J.S. and Yu X.L. Thermal fatigue on pistons induced by shaped high power laser. Part II: Design of spatial intensity distribution via numerical simulation. *International Journal of Heat and Mass Transfer* **51**(3-4) (2008), 768–778.
[16] Alimardani M., Toyserkani E. and Huissoon J.P. A 3D dynamic numerical approach for temperature and thermal stress distributions in multilayer laser solid freeform fabrication process. *Optics and Lasers in Engineering* **45**(12) (2007), 1115–1130.
[17] Sun P.P. Research on Microstructure and Properties of Hardened Layer by Laser Beams with Intensity Distributions. PhD thesis, Institute of Mechanics, Chinese Academy of Sciences. 2012.
[18] Tan Z. and Guo G.W. *Thermal Properties of Engineering Alloy*. Beijing: Metallurgical Industry Press. 1994.
[19] Zhang Y.J., Yu G., He X.L., Ning W.J. and Zheng C.Y. Numerical and experimental investigation of multilayer SS410 thin wall built by laser direct metal deposition. *Journal of Materials Processing Technology* **212**(1) (2012), 106–112.